2020

Demonstration of a Compliant Micro-Spring Array as a Thermal Interface Material for Pluggable Optoelectronic Transceiver Modules

J. Cui

L. Pan

J. A. Weibel

Jin Cui
School of Mechanical Engineering,
Purdue University,
West Lafayette, IN, 47906
e-mail: cui94@purdue.edu

Liang Pan[1]
School of Mechanical Engineering,
Purdue University,
West Lafayette, IN, 47906
e-mail: liangpan@purdue.edu

Justin A Weibel[1]
School of Mechanical Engineering,
Purdue University,
West Lafayette, IN, 47906
e-mail: jaweibel@purdue.edu

Demonstration of A Compliant Micro-Spring Array as A Thermal Interface Material for Pluggable Optoelectronic Transceiver Modules

Pluggable optoelectronic transceiver modules are widely used in the fiber-optic communication infrastructure. It is essential to mitigate thermal contact resistance between the high-power optical module and its riding heat sink in order to maintain the required operation temperature. The pluggable nature of the modules requires dry contact thermal interfaces that permit repeated insertion–disconnect cycles under low compression pressures (~10-100 kPa). Conventional wet thermal interface materials (TIM), such as greases, or those that require high compression pressures, are not suitable for pluggable operation. Here we demonstrate the use of compliant micro-structured TIM to enhance the thermal contact conductance between an optical module and its riding heat sink under a low compression pressure (20 kPa). The metallized and polymer-coated structures are able to accommodate the surface nonflatness and microscale roughness of the mating surface while maintaining a high effective thermal conductance across the thickness. This dry contact TIM is demonstrated to maintain reliable thermal performance after 100 plug-in and plug-out cycles while under compression.

Keywords: Pluggable optoelectronic transceiver module, Thermal interface material, Compliant micro-springs, Sliding contact

1 Introduction

Fiber-optic communication is a prevalent method of long-distance signal transmission [1, 2]. Pluggable optoelectronic transceiver modules [3] are used to convert light signals from an optical fiber to electrical signals. The current trends in miniaturization of the module form factors and high data bandwidths are leading to dramatically increasing power densities [4], which introduces new thermal management challenges to maintain operating temperatures [5-8]. The contact thermal resistance across the interface between the pluggable optical module and the riding heat sink surface constitutes a major portion of the total resistance to heat rejection.

Contact thermal resistances result from air gaps at the interface, which are formed by the mismatching microscale asperities (surface roughness) and wavy profiles (surface nonflatness) of the mating surfaces [9-11]. High compressive pressures can be applied on the interface to deform asperities and increase contact area; however, pressures as large as 1-100 MPa are necessary to effectively enhance contact thermal conductance across metal-to-metal interfaces [12-14], which is disallowed for pluggable optical modules. A common method to reduce contact thermal resistances under low pressures is to fill the air gaps with wet thermal interface materials (TIMs), such as greases and pastes [8]. These materials, which must be carefully applied to ensure complete wetting of the surfaces during compression, are not suitable for use in pluggable optical modules that must repeatedly slide into contact with the riding heat sinks.

There are various novel compliant TIMs that report promising thermomechanical performance [15-17]. Particle-laden polymers (PLPs) [18-21] combine the compliant mechanical properties of polymers and the high thermal conductance of filler particles. A higher filling ratio of particles leads to higher thermal conductance but sacrifices mechanical compliance [17]. Vertically aligned carbon nanotubes (CNTs) have extremely high axial thermal conductivity [22, 23] and can be bonded to mating surfaces to enhance contact thermal conductance [24, 25]. Metal nanowires [26, 27] and nanotubes [28, 29] having intrinsically high material thermal conductivity can be designed to have high mechanical compliance by engineering their shape/structure. These TIMs have reported extraordinary thermal performance, but permanent bonds must be created between the mating surfaces, which is not possible for pluggable optical modules.

Previously, we developed a compliant metallized micro-spring array as a TIM to enhance dry contact conductance under a low pressure of 20 kPa [30-32]. The polymer scaffolds that form the micro-springs are fabricated using a cost-effective, high-throughput projection micro-stereolithography (μSL) system. The polymer scaffold is then electrolessly plated with a high-thermal-conductivity metal layer. The metallized micro-spring array is demonstrated to conform to surface nonflatness on the order of 10s μm under low compressive pressures on the order of 10s kPa; this leads to a dramatic reduction in contact thermal resistance compared to a dry metal-to-metal interface without the TIM. However, a typical mating surface of a pluggable optical module has not only surface nonflatness, but also microscale surface roughness with asperities on the order of 1 μm or smaller. The larger-scale compliant micro-spring structure cannot deform to accommodate this microscale surface roughness.

In this work we demonstrate the use of polymer-coated metallized micro-structured TIM, which is capable of conforming to surface nonflatness and microscale roughness, to reduce the thermal interface resistance between an optical module and a heat sink. A commercially available C form-factor pluggable (CFP) optoelectronic transceiver module having a surface nonflatness of 10s μm and a surface roughness of 0.5 μm

[1]Corresponding authors.

is used for the demonstration. A thin layer of a soft polymer (polystyrene) is coated on the tops of metallized micro-springs to accommodate micro-roughness on the mating surface. The total insertion contact thermal resistance is measured when the dry TIM is placed between the surface of a CFP4 module and its riding heat sink under a compressive pressure of 20 kPa. Compared to the direct contact case, the contact thermal resistance is reduced by ~40% when the TIM is inserted. The short-term reliability is assessed by sliding the TIM across the mating surface of the optical module for 100 plug-in and plug-out cycles while under compression. There is no visible damage to the TIM or degradation in thermal performance after the cycles.

2 Methods

2.1 Micro-Structure Design. As shown in Fig. 1, the compliant micro-spring array is composed of many individual spring units having a so-called 'finned zig zag spring' geometry. The micro-spring array is composed of a polymer scaffold that is coated with a thermally conductive metal layer [30]. The finned zig zag spring has a symmetric shape comprising two basic springs elements arranged back to back. The top surfaces of these two spring elements are connected with a plate. The slots though the top plate are included to avoid a large, flat, and smooth surface, which would be hard to metallize without delamination. A series of 20-μm-thick fins are attached on the side walls of the springs, which increase the surface area for metallization to enhance the thermal conductance of the TIM. The total height of each finned zig zag spring is 440 μm, with footprint area of 700 μm × 580 μm. A 7 × 10 array of finned springs is arranged with a gap of 200 μm between neighboring springs in both directions. The dimensions of the base layer beneath the springs is 10 mm (L) × 6 mm (W) × 0.2 mm (H). Metal-coated through-holes (100 μm × 580 μm) near the feet of the micro-springs reduce the thermal resistance of the base layer [30].

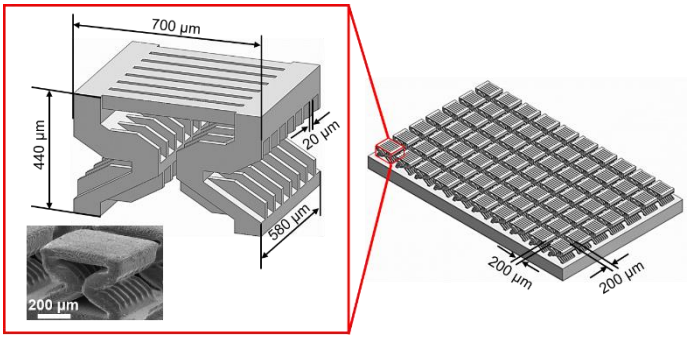

Fig. 1 Three-dimensional (3D) drawing of the micro-structured TIM. In the inset red frame are an enlarged view and scanning electron microscope (SEM) image of an individual finned zig zag micro-spring.

Figure 2 shows a schematic diagram of the interface cross section for the TIM when compressed between a pluggable optoelectronic transceiver module and the mating surface of a riding heat sink that has both surface nonflatness and micro-roughness. The micro-springs with lateral dimensions of 100s μm are able to accommodate surface nonflatness with 10s μm amplitude and 100s μm pitch. The thin layer of soft polymer is coated on top of the metallized micro-springs and can accommodate the surface roughness because it is easily deformed to fill the air gaps under low pressures. A thin layer of epoxy is applied between riding heat sink and the TIM to bond the surfaces and improve contact thermal conductance through this interface. Although the thermal conductivities of polymer and epoxy are low, the small thicknesses of the polymer (~0.5 μm) and epoxy (< 10 μm) layers do not impose a large thermal resistance.

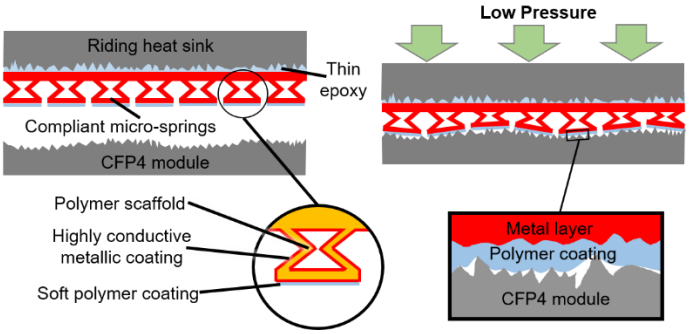

Fig. 2 Working mechanism of the compliant micro-spring array TIM. Compliant polymer-coated metallized micro-springs conformally contact a nonflat and rough mating surface when compressed at a low pressure. The micro-springs accommodate surface nonflatness while the soft polymer coating accommodates surface roughness.

2.2 Fabrication of the Metallized Micro-Spring Array. The polymer scaffolds of the TIM are fabricated using a custom projection micro-stereolithography (μSL) system [30-32]. This is a cost-effective and scalable additive manufacturing technology that can fabricate three-dimensional structures for various applications [33-36]. By using the projection method, this fabrication system has higher throughput and less stitching error than other 3D micro-fabrication techniques which use point-scanning methods [36, 37]. The system can build 3D structures at a speed of approximately 10 to 100 μm/s with a resolution better than 10 μm.

The polymer scaffold is electrolessly plated with a layer of copper (~2 μm thick) to enhance the effective thermal conductance of the structure [30]. A layer of nickel (~0.5 μm thick) is coated on the copper to protect from oxidation. The tops of the micro-springs are hand-polished to reduce the surface roughness of the metal layer.

2.3 Polymer Coating. A thin layer of polymer is coated on the metallized TIM to enhance the contact thermal conductance. The soft polymer can be deformed and fill the air gaps when lightly pressed against a rough mating surface. Polystyrene (PS; molecular weight ~300) grains are dissolved in chloroform

($CHCl_3$) by sonication to form a 0.5 wt% solution. The top surface of the metallized TIM is immersed in the PS solution and dried in a ventilation hood. The chloroform is allowed to evaporate at room temperature (~ 21 ℃), and the PS forms a thin layer of solid polymer on top of the TIM.

The Young's modulus and thickness of the PS coating are characterized by nanoindentation (Keysight G200). The nanoindentation test is performed on a polished nickel-coated copper plate with the PS layer applied using the same coating method; if performed directly on the micro-springs, their high mechanical compliance would confound the measurement. The Young's modulus is measured at different indentation depths at 25 different locations. The average modulus is 0.055 GPa at depth of 0.2 μm, which is 3 orders of magnitude lower than copper and nickel. When the indentation depth increases beyond ~0.5 μm, the modulus increases dramatically, which indicates that this is the thickness of polymer layer.

2.4 Thermal Demonstration using a Pluggable CFP4 Module. Figure 3 (a) shows a 3D drawing and critical dimensions of a commercially available pluggable optoelectronic transceiver module, specifically a CFP4 module. The top surface (enclosed by the dashed line) is the mating surface in contact with the riding heat sink. The mating surface has surface nonflatness of 10s μm and a surface roughness of 0.5 μm. An experimental setup is constructed to demonstrate the thermal performance of the TIM using the mating surface the CFP4 module, as shown in Fig. 3 (b). A tightly packed array of 2 × 12 fully-fabricated TIM micro-spring arrays are bonded upside down to the riding heat sink using thermal epoxy. The TIM-furnished heat sink is compressed against the mating surface of the module under a low pressure of 20 kPa. Heat generation in the module is simulated using heaters embedded underneath the mating surface. All other surfaces of the module are thermally insulated to minimize the heat loss. We assume that heat losses are negligible, such that all the heat generated is transferred through the TIM and dissipated by the heat sink. One thermocouple is set in a hole drilled into the heat sink and another thermocouple is embedded underneath the mating surface. The measured temperature difference between these thermocouples and the heating power are used to calculate the contact thermal resistance between the CFP4 module surface and heat sink.

2.5 Sliding Contact Cycling. For pluggable applications, the TIM needs to repeatedly slide into and out of contact with the module. Therefore, an experimental setup is built to characterize the sliding contact behavior of the TIM, as shown in Fig. 4. During the sliding contact test, the TIM is set on a platform and moved across the surface of the CFP4 module. The module surface is fixed on a kinetic platform; the TIM is fixed on a five-axis aligner. The kinetic platform and the five-axis aligner together ensure parallel motion between the module surface and the TIM. A horizontal linear stage and a motorized translation stage are used to control the position and motion of the TIM. The desired compressive pressure is set by moving the vertical translation stage and measuring the force by a load cell located under the TIM plate (Load cell 1). The shear force applied by moving the motorized translation stage is measured by a load cell fixed to the CFP4 module surface (Load cell 2).

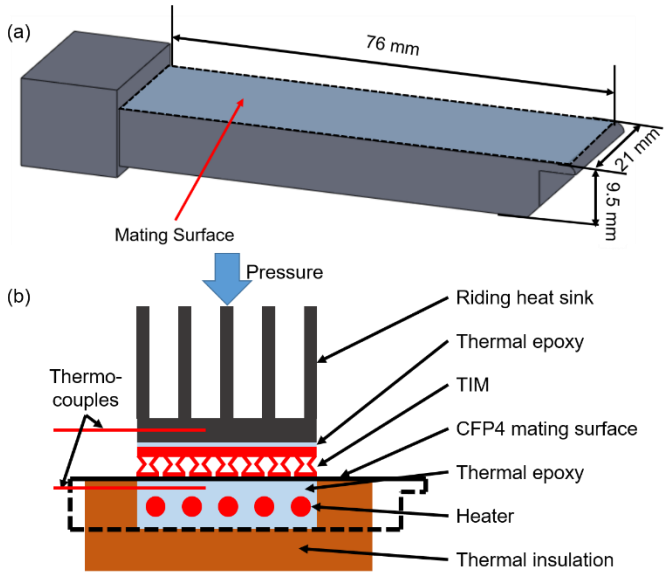

Fig. 3 (a) 3D drawing of a CFP4 module. The dashed line indicates the mating surface. (b) Schematic illustration of the experimental setup constructed to demonstrate the thermal performance of the dry TIM using the mating surface of the CFP4 module. The dashed line indicates the outer shell of the CFP4 module, on which the riding heat sink is pressed down on from above.

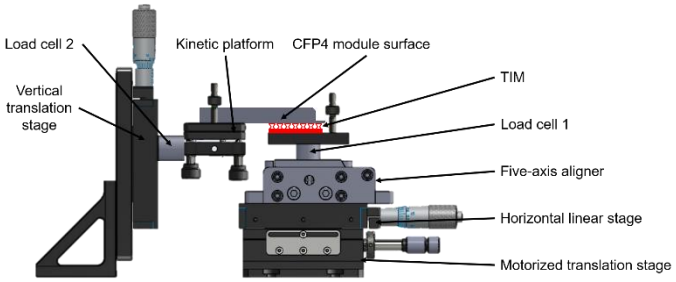

Fig. 4 Experimental setup used to characterize the behavior of the TIM when sliding against a CFP4 module surface.

3 Results

3.1 Thermal Resistances of TIMs with Different Coatings in Contact with a Rough Surface. To evaluate the influence of the polymer coating on the TIM thermal resistance when contacting a rough surface, we consider a mating surface with a milled finish, as shown in the inset image in Fig. 5. There are approximately 100 scratches per millimeter on the surface, which has a roughness of 0.52 μm characterized by an optical

interferometer (Zygo NewView 6200). The surface also has a surface nonflatness of 10s µm, which can be compensated by the structural compliance. Using an experimental setup which characterizes contact thermal resistance by one-dimensional steady state heat transfer, as described in detail in Ref. [30], the thermal resistances of the metallized TIM with and without polymer coatings are evaluated under a normal pressure of 20 kPa; these resistances are compared to the thermal resistance of direct metal-to-metal contact in Fig. 5. The direct metal-to-metal contact thermal resistance is 1280 ± 40 mm^2·K/W, while the thermal resistance of the metallized TIM (without the polymer coating) is 550 ± 30 mm^2·K/W. The metallized TIM outperforms direct metal-to-metal contact because the compliant micro-springs can conform to the surface nonflatness. After polymer coating, the thermal resistance of the TIM is further reduced to 350 ± 20 mm^2·K/W. This indicates that the soft polymer coating conforms to surface roughness; the benefit of increased contact area outweighs the thermal conduction resistance across the layer thickness.

3.2 Polymer-Coated Metallized TIM Thermal Demonstration. A thermal demonstration using the CFP4 module is conducted with a step input heating power of 5 W under a pressure of 20 kPa. The performance with the polymer-coated metallized TIM is compared to a case where the mating surface directly contacts the riding heat sink, without any TIM inserted. The temperatures of the heat sink and CFP4 module are shown with time in Fig. 6 (a). The zero time is aligned with the instant that the heater is turned on. The steady state heat sink temperatures are almost same for both cases because the ambient temperature is the same (~21 ℃). The temperature of the CFP4 module, which depends on the thermal resistance across the interface, is lowered with the TIM inserted.

The total insertion thermal resistance is estimated based on the temperature difference and the heating power; the calculated values are shown in Fig. 6 (b). The direct contact insertion thermal resistance is 620 ± 60 mm^2·K/W, while the total insertion resistance of the polymer-coated metallized TIM is 390 ± 45 mm^2·K/W, which is 40% lower than direct contact. The results demonstrate that the TIM enhances the contact thermal conductance and lowers the operating temperature of the CFP4 module. Note that the total insertion thermal resistance of the TIM here is higher than that reported for the rough surface in Fig. 5 because of additional resistances included in the calculation of the total insertion resistance (namely, due to conduction through the mating surface, a small portion of heat sink, and across the epoxy interface underneath the TIM).

3.3 Performance and Reliability under Sliding Contact. The polymer-coated metallized TIM is moved against a CFP4 module surface at a speed of 5 mm/s for a distance of 5 mm to characterize its resilience during sliding contact. The measured normal force and shear force applied to the TIM during a single sliding contact test are shown in Fig. 7 (a). Both the normal force and shear force remain nearly constant during sliding. The average normal force is 1.20 N, corresponding to a compressive pressure of 20 kPa; the average shear force is 0.19 N, which corresponds to a friction factor of 0.16.

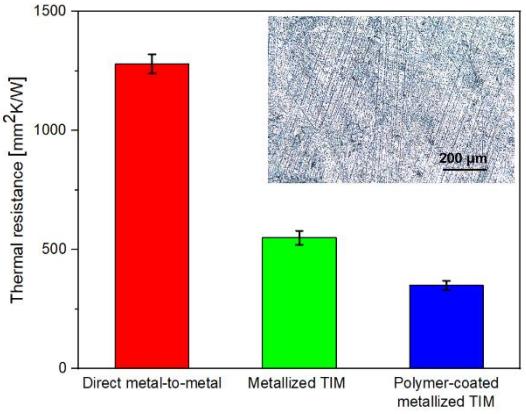

Fig. 5 Comparison of thermal resistances of dry metal-to-metal contact without the TIM, with the metallized TIM, and with the polymer-coated metallized TIM. Inset is the optical microscopic image of the rough (~0.5 µm) surface fabricated by milling.

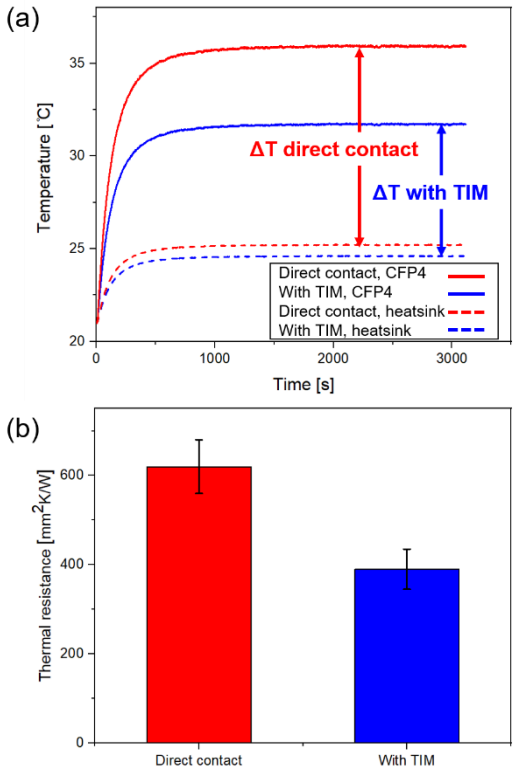

Fig. 6 (a) Temperatures of the CFP4 module and heat sink with time after the step heat input; cases are shown with and without the polymer-coated metallized TIM inserted in the interface. (b) The total insertion thermal resistances with and without the TIM inserted.

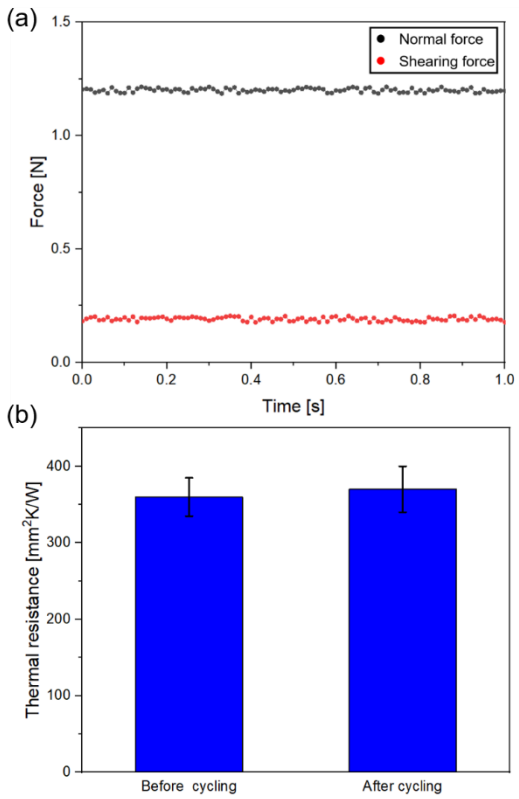

Fig. 7. (a) Measured normal and shear force applied on the polymer-coated metallized TIM during sliding contact tests. (b) Thermal resistance of the TIM measured before and after 100 sliding contact cycles.

To evaluate the reliability of TIM under sliding contact, the polymer-coated metallized TIM is repeatedly moved back and forth across the surface for 100 cycles, maintaining contact with the module surface under a compressive pressure of 20 kPa. Based on visual inspection, the TIM does not have any obvious damage after cycling. The thermal resistance of the TIM before and after sliding contact cycling is characterized under pressure of 20 kPa by using the rough surface shown in Fig. 5 as the mating surface. As shown in Fig. 7 (b), the thermal resistance of the polymer-coated metallized TIM is almost the same before and after sliding (difference within the measurement uncertainty). The TIM can survive repeated plug-in and plug-out cycles without thermal performance degradation.

4 Conclusions

We demonstrate a polymer-coated metallized micro-spring array as a dry thermal interface material (TIM) for pluggable optoelectronic transceiver modules. The metallized micro-spring array has been previously demonstrated to effectively enhance dry contact thermal conductance with nonflat mating surfaces. To accommodate microscale surface roughness, we coat a thin layer of soft polymer on the metallized TIM. Thermal resistance characterization using rough mating surfaces (~0.5 μm) confirms that this polymer coating conforms to surface roughness and reduces the thermal resistance under a compressive pressure of 20 kPa. The polymer-coated metallized TIM is then demonstrated to enhance the contact thermal conductance between a CFP4 module mating surface and its riding heat sink. The thermal and mechanical reliability of the TIM is evaluated by sliding the TIM against a CFP4 module surface for 100 cycles at the compressive pressure required of pluggable applications.

Acknowledgments

Financial support for this work was provided by members of the Cooling Technologies Research Center (CTRC), a graduated National Science Foundation Industry/University Cooperative Research Center at Purdue University, and the National Science Foundation (Grant No. CMMI-1554189 and CMMI-1634832).

References

[1] Keiser, G., 2003. Optical fiber communications. Wiley Encyclopedia of Telecommunications.

[2] Agrawal, G.P., 2012. Fiber-optic communication systems (Vol. 222). John Wiley & Sons.

[3] Implementation Agreement for Thermal Interface Specification for Pluggable Optics Modules, 2015, Optical Internetworking Forum, OIF-Thermal-01.0.

[4] Sheltami K and Refai-Ahmed G., 2002. “Thermal management of telecommunication optical module in forced convection mode.” In: ITherm 2002 Eighth Intersociety Conference on Thermal and Thermomechanical Phenomena in Electronic Systems. p. 726–729.

[5] Marotta, E. E., and Hana, B., 1998, “Thermal control of interfaces for microelectronic packaging,” MRS Online Proceedings, Library Archive 515.

[6] Atluri, V.P., Mahajan, R.V., Patel, P.R., Mallik, D., Tang, J., Wakharkar, V.S., Chrysler, G.M., Chiu, C.P., Choksi, G.N. and Viswanath, R.S., 2003, “Critical aspects of high-performance microprocessor packaging,” MRS Bulletin, 28(1), pp. 21-34.

[7] Garimella, S.V., Fleischer, A.S., Murthy, J.Y., Keshavarzi, A., Prasher, R., Patel, C., Bhavnani, S.H., Venkatasubramanian, R., Mahajan, R., Joshi, Y. and Sammakia, B., 2008, “Thermal challenges in next-generation electronic systems,” IEEE Transactions on Components and Packaging Technologies, 31(4), pp.801-815.

[8] Prasher, R., 2006, “Thermal interface materials: historical perspective, status, and future directions,” Proceedings of the IEEE, 94(8), pp.1571-1586.

[9] Cooper, M.G., Mikic, B.B. and Yovanovich, M.M., 1969, “Thermal contact conductance,” International Journal of Heat and Mass Transfer, 12(3), pp.279-300.

[10] Madhusudana, C.V. and Ling, F.F., 1996, Thermal Contact Conductance (pp. 1-43), New York: Springer-Verlag.

[11] Yeh, L.T. and Chu, R.C., 2002, Thermal Management of Microelectronic Equipment, New York: ASME.

[12] Antonetti, V.W., and Yovanovich, M.M., 1985, “Enhancement of thermal contact conductance by metallic coatings: theory and experiment,” Journal of Heat Transfer, 107(3), pp.513–519.

[13] Lambert, M.A. and Fletcher, L.S., 1993, “Review of the thermal contact conductance of junctions with metallic coatings and

films," Journal of Thermophysics and Heat Transfer, 7(4), pp.547-554.
[14] Merrill, C.T. and Garimella, S.V., 2011, "Measurement and prediction of thermal contact resistance across coated joints," Experimental Heat Transfer, 24(2), pp.179-200.
[15] Bar-Cohen, A., Matin, K. and Narumanchi, S., 2015, "Nanothermal interface materials: Technology review and recent results," Journal of Electronic Packaging, 137(4), p.040803.
[16] McNamara, A.J., Joshi, Y. and Zhang, Z.M., 2012, "Characterization of nanostructured thermal interface materials – A review," International Journal of Thermal Sciences, 62, pp.2-11.
[17] Hansson, J., Nilsson, T.M., Ye, L. and Liu, J., 2017, "Novel nanostructured thermal interface materials: A review," International Materials Reviews, 63(1), pp.22-45.
[18] Ishida, H. and Rimdusit, S., 1998, "Very high thermal conductivity obtained by boron nitride-filled polybenzoxazine," Thermochimica Acta, 320 (1), pp.177–186.
[19] Lin, W., Moon K., and Wong, C.P., 2009, "A combined process of in situ functionalization and microwave treatment to achieve ultrasmall thermal expansion of aligned carbon nanotube–polymer nanocomposites: Toward applications as thermal interface materials," Advanced Materials, 21(23), pp.2421–2424.
[20] Shahil, K.M.F., and Balandin, A.A., 2012, "Thermal properties of graphene and multilayer graphene: Applications in thermal interface materials," Solid State Communications, Exploring Graphene, Recent Research Advances, 152 (15), pp.1331–1340.
[21] Pashayi, K., Fard, H.R., Lai, F., Iruvanti, S., Plawsky, J., and Borca-Tasciuc, T., 2014, "Self-constructed tree-shape high thermal conductivity nanosilver networks in epoxy," Nanoscale, 6 (8), pp.4292–4296.
[22] Iijima, S., 1991, "Helical microtubules of graphitic carbon," Nature, 354, pp.56-58.
[23] Marconnet, A.M., Panzer, M.A. and Goodson, K.E., 2013, "Thermal conduction phenomena in carbon nanotubes and related nanostructured materials," Reviews of Modern Physics, 85(3), p.1295.
[24] Wasniewski, J.R., Altman, D.H., Hodson, S.L., Fisher, T.S., Bulusu, A., Graham, S. and Cola, B.A., 2012, "Characterization of metallically bonded carbon nanotube-based thermal interface materials using a high accuracy 1D steady-state technique," Journal of Electronic Packaging, 134(2), p.020901.
[25] Lin, W., Zhang, R., Moon, K.S. and Wong, C.P., 2010, "Synthesis of high-quality vertically aligned carbon nanotubes on bulk copper substrate for thermal management," IEEE Transactions on Advanced Packaging, 33(2), pp.370-376.
[26] Feng, B., Faruque, F., Bao, P., Chien, A., Kumar, S., and Peterson, G. P., 2013, "Double-sided tin nanowire arrays for advanced thermal interface materials," Applied Physics Letters, 102 (9), pp.093-105.
[27] Barako, M.T., Roy-Panzer, S., English, T.S., Kodama, T., Asheghi, M., Kenny, T.W. and Goodson, K.E., 2015, "Thermal conduction in vertically aligned copper nanowire arrays and composites," ACS Applied Materials & Interfaces, 7 (34) pp.19251–19259.
[28] Shaddock, D., Weaver, S., Chasiotis, I., Shah, B. and Zhong, D., 2011. "Development of a compliant nanothermal interface material," ASME InterPack, IPACK2011, Portland, Oregon, USA, pp.13-17.
[29] Kempers, R., Lyons, A.M. and Robinson, A.J., 2014, "Modeling and experimental characterization of metal microtextured thermal interface materials," Journal of Heat Transfer, 136(1), p.011301.
[30] Cui, J., Wang, J., Weibel, J.A. and Pan, L., 2019. A compliant microstructured thermal interface material for dry and pluggable interfaces. International Journal of Heat and Mass Transfer, 131, pp.1075-1082.
[31] Cui, J., Wang, J., Zhong, Y., Pan, L., Weibel, J.A., 2018, "Metallized compliant three-dimensional microstructures for dry contact thermal conductance enhancement," Journal of Micromechanics and Microengineering 28 (5) p.055005.
[32] Wasielewski, R., Cui, J., Pan, L., Weibel, J. A., 2016, "Fabrication of compliant three-dimensional microstructures as surface coatings for dry contact thermal conductance enhancement." 15th IEEE Intersociety Conference on Thermal and Thermomechanical Phenomena in Electronic Systems (ITherm), Las Vegas, Nevada, USA, pp.134–39.
[33] Sun, C., Fang, N., Wu, D.M. and Zhang, X., 2005, "Projection micro-stereolithography using digital micro-mirror dynamic mask," Sensors and Actuators A: Physical, 121(1), pp.113-120.
[34] Zheng, X., Deotte, J., Alonso, M.P., Farquar, G.R., Weisgraber, T.H., Gemberling, S., Lee, H., Fang, N. and Spadaccini, C.M., 2012, "Design and optimization of a light-emitting diode projection micro-stereolithography three-dimensional manufacturing system," Review of Scientific Instruments, 83(12), p.125001.
[35] Bao, Y., He, C., Zhou, F., Stuart, C. and Sun, C., 2012, "A realistic design of three-dimensional full cloak at terahertz frequencies," Applied Physics Letters, 101(3), p.031910.
[36] Lin, D., Nian, Q., Deng, B., Jin, S., Hu, Y., Wang, W. and Cheng, G.J., 2014, "Three-dimensional printing of complex structures: man made or toward nature?" ACS Nano, 8(10), pp.9710-9715.
[37] Meza, L.R., Das, S. and Greer, J.R., 2014, "Strong, lightweight, and recoverable three-dimensional ceramic nanolattices," Science, 345(6202), pp.1322-1326.
[38] Soukoulis, C.M. and Wegener, M., 2011, "Past achievements and future challenges in the development of three-dimensional photonic metamaterials," Nature Photonics, 5(9), pp.523-530.